Structure of the Cytosolic Part of the Subunit *b*-Dimer of *Escherichia coli* F_0F_1-ATP Synthase

Tassilo Hornung, Oleg A. Volkov, Tarek M. A. Zaida, Sabine Delannoy, John G. Wise, and Pia D. Vogel
Department of Biological Sciences, Southern Methodist University, Dallas, Texas

ABSTRACT The structure of the external stalk and its function in the catalytic mechanism of the F_0F_1-ATP synthase remains one of the important questions in bioenergetics. The external stalk has been proposed to be either a rigid stator that binds F_1 or an elastic structural element that transmits energy from the small rotational steps of subunits *c* to the F_1 sector during catalysis. We employed proteomics, sequence-based structure prediction, molecular modeling, and electron spin resonance spectroscopy using site-directed spin labeling to understand the structure and interfacial packing of the *Escherichia coli b*-subunit homodimer external stalk. Comparisons of bacterial, cyanobacterial, and plant *b*-subunits demonstrated little sequence similarity. Supersecondary structure predictions, however, show that all compared *b*-sequences have extensive heptad repeats, suggesting that the proteins all are capable of packing as left-handed coiled-coils. Molecular modeling subsequently indicated that b_2 from the *E. coli* ATP synthase could pack into stable left-handed coiled-coils. Thirty-eight substitutions to cysteine in soluble *b*-constructs allowed the introduction of spin labels and the determination of intersubunit distances by ESR. These distances correlated well with molecular modeling results and strongly suggest that the *E. coli* subunit *b*-dimer can stably exist as a left-handed coiled-coil.

INTRODUCTION

F_0F_1-ATP synthases are ubiquitous enzymes that are responsible for the bulk of ATP production during oxidative or photophosphorylation in aerobic organisms. These highly asymmetric enzymes use the energy inherent in proton gradients across energy-coupling membranes, such as the inner mitochondrial membrane, the thylakoid membrane of plants, or the plasma membrane of bacteria, to form a high-energy anhydride bond during the synthesis of ATP. One of the simplest members of the ATP synthase family is found in the bacterium *Escherichia coli*. The membrane sector of this synthase consists of three types of subunits, subunit-*a*, -*b*, and -*c*, with a stoichiometry of $ab_2\ c_{10\text{-}15}$. The membrane-associated F_1-part of the synthase is only capable of net ATP-hydrolysis when dissociated from the membrane. It consists of five different subunits in the stoichiometry $\alpha_3\beta_3\gamma\delta\varepsilon$. Three of the six total nucleotide sites are the sites of ATP synthesis or hydrolysis. These catalytic sites are present mainly on the β-subunits. The function of the three noncatalytic sites remains unclear.

Proton translocation is catalyzed by a concerted action of subunits *a* and *c* that drives a rotary motion of the *c*-ring. This rotation is transmitted to the internal stalk, which consists of subunits γ and ε. Asymmetric interaction of the rotating subunit γ with the nucleotide binding sites then results in conformational transitions within the catalytic sites that enable ATP that has spontaneously formed in the tight catalytic site to be released (for earlier reviews, see Boyer (1), Senior et al. (2), and Yoshida et al. (3)). The concerted movement of the internal stalk of F_1 with the ring of subunits *c* of F_0 relative to the hexameric ring of subunits α and β implies the structural necessity of a second stalk that functions as a stator during rotational catalysis. Convincing evidence has been provided that this second stalk corresponds in bacteria and plants to a dimer of subunit *b* and the δ-subunit of F_1 (4–7). Subunit *a* of F_0 also appears to be part of the stator and is positioned externally to the ring of *c*-subunits.

Evidence has been provided that demonstrated interactions of subunit *a* with the *c*-ring and the *b*-dimer (8–12). Rotation of subunits *c*, γ, and ε has been suggested to generate elastic torque within the internal and external stalks that needs to be stored or transferred to other subunits via concerted conformational changes (13,14). Gaining new knowledge on the structure of the stator subunits and their protein-protein interactions is therefore of great importance for understanding the mechanism of energy transduction within the synthase. X-ray structural models of substructures of ATP synthases from different organisms have been available for some time (15–20). In addition, NMR and x-ray structural data are available for the smaller subunits ε and δ (21–23). Structural information on subunit *a* has so far been limited to mutational analysis, chemical modification, and limited proteolysis (for example, see Zhang and Vik (24)).

The *E. coli* subunit *b* forms a homodimeric structure with a highly hydrophobic N-terminal region that likely serves as a membrane anchor (25). The remaining amino acids are predicted to form extended α-helices with some portions interacting

Submitted August 30, 2007, and accepted for publication January 29, 2008.

Address reprint requests to Pia D. Vogel, Dept. of Biological Sciences, Southern Methodist University, Dallas, TX, Tel.: 214-768-1790; Fax: 214-768-3955; E-mail: pvogel@smu.edu.

Tassilo Hornung's present address is Biomedicine and Biotechnology, School of Life Sciences, Arizona State University, Tempe, AZ.

Sabine Delannoy's present address is Agence Française de Sécurité Sanitaire des Aliments, Maisons-Alfort, France.

Editor: David D. Thomas.

0006-3495/08/06/5053/12 $2.00

doi: 10.1529/biophysj.107.121038

with F_1. Ultracentrifugation and circular dichroism analyses have suggested that coiled-coil packing would dominate *b*-dimerization interactions (26–29). The structure of the membrane domain of the *b*-subunit (residues 1–34) has been solved using NMR spectroscopy (30), and the expression of a truncated, water-soluble subunit *b* has allowed studies of its dimerization properties (26–28,31; for reviews, see Dunn et al. (32) and Dunn et al. (33)). In addition, an x-ray crystallographic structure of a monomeric version of a 60-residue truncated subunit *b* has been published (34). A slight right-handed twist of the putative dimerization surface of *b* was used as suggestive evidence to infer that the *b*-dimer packs in a right-handed coiled-coil dimer (34), an unusual quaternary structure that has not yet been directly observed.

The results of studies of disulfide formation at cysteines introduced at asymmetrical positions within the *b*-sequence were used as additional evidence for a right-handed coiled-coil form for the *b*-dimer (35). To accommodate the observations of disulfide bonds at nonhomologous (''staggered'') positions in subunit *b* and the undecad repeat sequence that is supportive of right-handed coiled-coil, also identified by these authors, a staggered dimer with an interaction surface offset by at least four residues was proposed (35). A putative offset of 27 Å of the *b* helices was also suggested as one potential model to accommodate interhelical distances obtained by double electron-electron resonance electron spin resonance (ESR) measurements of site-specifically spin-labeled amino acids in the tether domain of subunit *b* in reconstituted *E. coli* F_0F_1-ATP synthase (36). How these staggers and offsets can be accommodated with the nonstaggered transmembrane anchors of the *E. coli* homodimeric subunit *b* remains unclear at this time, however.

Deletions of up to 11 residues and insertions of up to 14 amino acids in the bacterial *b*-dimer have been constructed that retained biological activity (37,38), suggesting relatively large flexibility in the structure of *b*. Constructs where *b*-subunits of unequal lengths have been coexpressed also resulted in the assembly of catalytically active F_0F_1-ATPase (39–41). The finding that parts of the tether domain of *b* (excluding those parts that apparently interact with the F_1-ATPase) could be exchanged for sequences stemming from cyanobacterial ATP synthase *bb′*-subunits suggested that there is limited, but required specificity in protein-protein interaction (42). Although the data obtained from work on bacterial ATPases seem to suggest relatively high flexibility of the *b*-subunit dimer, both in length and in sequence requirements, the recent x-ray structural model of the mitochondrial external stalk alternatively suggests a very rigid organization (43). Mitochondrial ATPases contain only a single copy of subunit *b*, which is supplemented by single copies of the subunits *F6* and *d*. The C-terminal end of *b* interacts with oligomycin sensitivity-conferring protein, the mitochondrial homolog to bacterial subunit δ. The x-ray structure of just subunits *b*, *F6*, and *d* showed a pronounced curvature that seems to perfectly accommodate binding to the F_1-ATPase (for recent reviews, see Walker and Dickson (44), Weber (45), and Weber (46)).

One important function of the subunit *b*-dimer seems to be to tether the $\alpha_3\beta_3$-subunit ring to F_0, which was indicated by the finding that the binding affinity of subunit δ to δ-depleted F_1 increases ~500-fold in the presence of *b*-dimer, providing additional binding energy of more than 15 kJ/mol (47). This additional binding energy has been suggested to be enough for *b* to function as a stator (47). Work from our lab has shown that *b*-dimer binding strongly influenced the conformation of the catalytic sites in F_1, rendering a larger population of catalytic sites in a more open conformation (48). We were also able to map the interaction of the *b*-dimer with soluble F_1 and showed that *b* bound to δ-depleted F_1 in a different conformation than observed with δ-replete enzyme (49).

We and others have employed ESR spectroscopy with the use of stable nitroxide radicals to extensively study proteins and enzymes, including F_1-ATPases from different organisms. Either the stable radicals employed can be linked to enzyme substrates (50–60; for reviews see Trommer and Vogel (61) and Vogel (62)) or they may be introduced by cysteine-specific spin labeling (63,64). The use of these probes has allowed the observation of conformational transitions upon protein-protein interactions, during catalytic turnover as well as protein-dynamic events.

In the work described here, 38 single cysteine mutations were introduced into *E. coli* subunit *b*, which were then chemically modified with cysteine-reactive spin labels. The use of the often employed cysteine-specific methanethiosulfonate spin label (MTS-SL) and the acquisition of the ESR spectra in frozen solution allowed us to determine interspin distances through evaluation of dipolar line broadening of the resulting spectra. The distances obtained from spin labels introduced at the same amino acid positions along the *b*-dimer correlated well with the distances obtained for left-handed coiled-coil molecular models of the subunit *b*-dimer. The propensity to form left-handed coiled-coil structures was investigated for bacterial, cyanobacterial, and plant *b*-subunits and *b*-subunit homologous proteins. Our results strongly suggest that *b*-dimers can fold into stable, left-handed coiled-coils.

MATERIALS AND METHODS

Mutagenesis and expression of subunit *b*

The single cysteine mutations of subunit *b* were obtained by standard molecular biology techniques and as described here. Cysteine mutations of the truncated subunit *b*-dimer were expressed in *E. coli* strain JM109. For easier purification, a vector was created based on the previously published pDM3 (31) that included a C-terminal His-10-tag sequence. This plasmid was used for the creation and expression of new mutations or for the expression of previously generated *b*-mutations recloned from pDM3 with *Eco*RI and *Sac*I.

Purification and chemical modification of subunit *b*

Truncated single cysteine mutations of *b*-dimer without His-tags were purified as described (31). The protein-containing fractions were assayed for protein content using the Bradford technique (65) and were pooled and concentrated to 3–5 ml using Amicon ultraconcentrators equipped with PM-10 membranes (Millipore, Bedford, MA). The protein was then aliquoted and stored at −80°C. Alternatively, the His-tagged proteins were applied to nickel-nitrilotriacetic acid agarose column in a buffer containing 50 mM TrisHCl, 100 mM NaCl, 30 mM imidazole, 1 mM dithiothreitol, pH 8.2. Protein was eluted with the same buffer supplemented with 250 mM imidazole. The protein-containing fractions were pooled and concentrated using Centricon-10 microconcentrators (Millipore).

For chemical modification, the proteins were transferred into a buffer consisting of 50 mM TrisHCl, 5 mM $MgSO_4$, pH 7.5 with either 300 mM KCl or 10 mM KCl. Buffer change was accomplished by passage of the proteins through a Sephadex G-25 column (Roche, Basle, Switzerland) equilibrated with the desired buffer. The protein-containing fractions were again pooled and concentrated to 2–3 ml using Centricon-10 microconcentrators. Protein concentration was determined using the Bradford method (65). The samples were then incubated for 30–60 min at 4°C or 20°C with 4-(2-iodoacetamido)-2,2,6,6-tetramethylpiperidine 1-oxyl (IAAT) or (1-oxyl-2,2,5,5-tetramethyl-3-pyrroline-3-methyl) MTS-SL (100 mM in acetonitrile or dimethyl sulfoxide) at a 5- to 10-fold molar excess of spin label over *b*-dimer. Excess spin label was removed with the same column system as in the previous step. The modified *b*-dimer fractions were concentrated in Centricon-10 microconcentrators and were stored at −80°C. Protein purity was verified using sodium dodecyl sulfate polyacrylamide gel electrophoresis (66). IAAT spin label was purchased from Sigma (St. Louis, MO). MTS-SL was a generous gift from Kalman Hideg, Hungary, or purchased from Toronto Research Chemicals (Toronto, Canada). Typical concentrations of spin-labeled *b*-subunits were between 20 and 100 μM. The extent of spin labeling was assayed by double integration of the resulting ESR spectra and was typically >80%.

ESR spectroscopy

ESR spectra were acquired at a Bruker ESP-300 E equipped with a dielectric cavity TE001 or a Bruker EMX 6/1, either equipped with a dielectric cavity TE001 or a high sensitivity cavity (Bruker, Billerica, MA). All spectra were acquired in the X-band mode with a peak-to-peak modulation amplitude of 1 G. The receiver gain was adjusted to the protein concentrations and the degree of labeling of the samples. The microwave power was 12.5 mW, and the spectra were acquired at 193 K or 223 K. The buffer used for ESR spectroscopy was 50 mM TrisHCl, 5 mM $MgSO_4$, and 300 mM KCl, pH 7.5 or 50 mM TrisHCl, 5 mM $MgSO_4$, and 10 mM KCl. ESR spectra were recorded in either the presence or absence of 20% (v/v) glycerol. The spectra were analyzed using a convolution algorithm assuming a Gaussian distribution of distances as previously described in detail in Hustedt et al. (67), and that was developed according to the procedures described in Rabenstein and Shin (68) and Steinhoff et al. (69).

Modeling the spin-labeled cysteinyl residue

The structure of the IAAT spin-labeled cysteine residue, and the MTS-SL cysteine residues were drawn using Molecular Simulations InsightII program (v. 2000.1; Insight Interactive, Rocky Hill, CT). Quantum mechanical simulations of the spin-labeled derivatized cysteinyl residues to locate equilibrium geometries were performed using the program GAMESS (70), employing an unrestricted Hartree-Fock 6-31 basis set. The calculation of a Hessian matrix on the minimized structures allowed deduction of partial atomic charges for the residues. The program MOLDEN (G.Schaftenaar, Centre for Molecular and Biomolecular Informatics, Nijmegen, The Netherlands) was used for visualization of the quantum mechanics-/molecular mechanics-derived structures (71). Parameters and topology files were created using these data and by analogy to the work of Fajer and co-workers (72). All hydrogens were included in the simulations and parameterizations. Solvent-accessible surface representations were calculated by the MSMS program described in Sanner et al. (73).

Modeling of the *b*-dimer coiled-coil domain

The *E. coli* ATP synthase *b*-dimer coiled-coil domains were modeled as described (Wise and Vogel, preceding article). Prediction of heptad repeats in the subunit *b* amino acid sequence was performed with the Paircoil2 program (74) using a sequence window size of 28 residues or the Multicoil program (75). The Visual Molecular Dynamics (VMD) suite of programs (76) was extensively used for the visualization and analysis of protein structures. The extraction of distance and dihedral data from known protein structures was performed using the Tcl/Tk (77) and Python (78) scripting interfaces incorporated into the VMD graphical user interface. Briefly, seven known left-handed, dimeric coiled-coil entries in the Protein Data Bank were analyzed within their coiled-coil domains with the Paircoil2 program and Tcl-scripts run in the VMD program to generate a set of ideal distance and dihedral restraints for dimeric left-handed coiled-coil domains. These ideal restraints between homologous heptad positions between Cα atoms were calculated and averaged and then applied to the subunit *b* heptad positions predicted by Paircoil2 to generate distance restraint tables for homologous interchain Cα atoms. In addition to these Cα distance restraints, ϕ and ψ dihedral angle and long-range intrasubunit distance restraints were employed.

The ideal distance and angle restraint tables generated for the subunit *b*-sequence were then used in ab initio simulated annealing (SA) experiments with the XPLOR-NIH suite, versions 2.11–2.18 (79) as described in Wise and Vogel (preceding article). These experiments generated left-handed coiled-coil structures for subunit *b* between residues 31 and 122. Initial models were refined, and a subset of acceptable structures was identified. Where appropriate, specific residues of subunit *b* were individually substituted with the spin-labeled cysteine residue, and additional ab initio SA calculations with the modified residue and restraint data corresponding to ESR distance measurements were performed. These experiments were either independent models generated (Wise and Vogel, preceding article) or used the backbone Cα atom positions fixed to the positions identified in the best model for the underivatized subunit *b*-dimer.

The computers used were Intel Pentium P4 32-bit single CPU units running OpenSuse10 or Scientific Linux 5.0 and a 44-CPU Linux computing cluster with either Scientific Linux 5.0 or FedoraCore 4 Linux operating systems.

RESULTS

Sequence alignment of *b*-subunits

We used the multiple sequence alignment program ClustalW (80) to align 53 subunit *b*-sequences and *b*-homologous subunits selected from bacteria, cyanobacteria, and flowering plants. The results were visualized with Jalview version 2.2.1 (81) and are shown in Fig. 1. The sequence numbers given at the top of Fig. 1 correspond to the *E. coli* subunit *b* numbering. The sequence for *E. coli b* is emphasized, as is the sequence of subunit *b* of the cyanobacterium *Synechocystis* sp. PCC 6803, which is also studied in our lab. The different origins of the subunits are listed in Table 1. It is clear from Fig. 1 that very little sequence similarity exists among the various members of the *b*-protein family with only a very limited number of identifiable conserved amino acids. This observation is

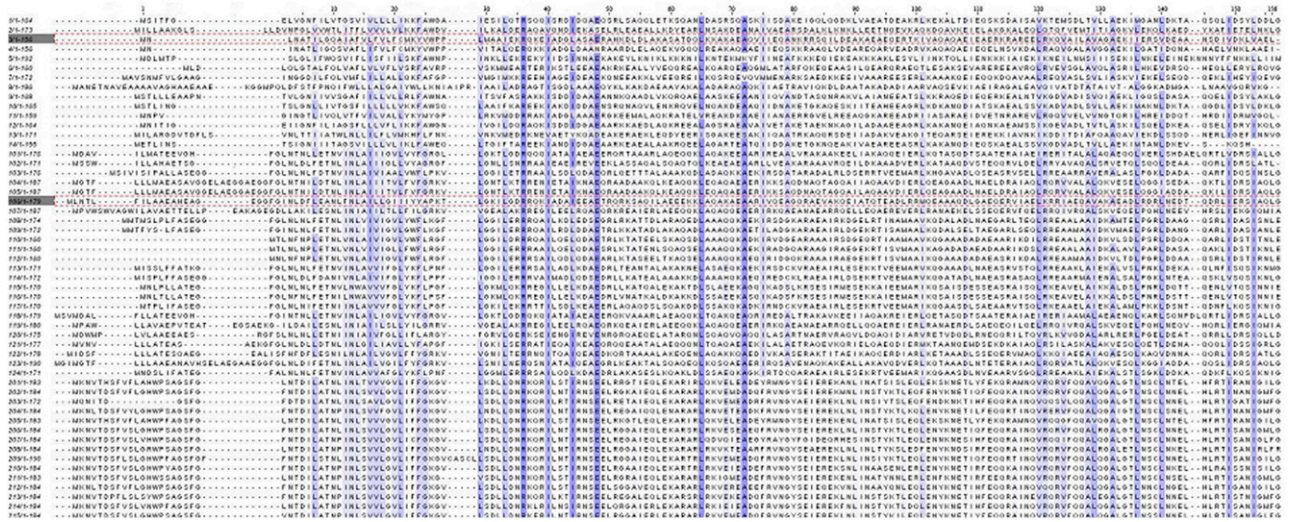

FIGURE 1 Sequence similarity prediction of *b*-subunits. Arbitrarily selected *b*-subunit sequences of bacterial, cyanobacterial, and plant F_0F_1-ATP synthases were aligned using the ClustalW alignment series (78). Different degrees of amino acid identity or homology are implied by different shades of coloring. For better legibility, the sequences in the figure were truncated after the last *E. coli* amino acid.

consistent with a structural role for the *b*-subunits within the overall F_0F_1-ATPase complex that does not require distinct amino acid interactions at defined positions for catalytic process to occur. It is to be expected, however, that if the *b*-subunits are to play similar structural roles in the different ATPases, the different sequences should be able to adopt similar overall protein structures.

Structure prediction of coiled-coil formation for *E. coli b* and other *b*-like proteins

Since it had been suggested earlier and prior experimental support had been provided that *b*-subunits exist as elongated, dimeric, α-helical structures, we employed the improved structure prediction program Paircoil2 (74). Paircoil2 was developed to identify residues that have a high probability of being in a heptad repeat. Left-handed coiled-coils are defined by repeating units of seven amino acids (heptad repeats) with a general requirement for apolar residues at the first and fourth heptad positions *A* and *D* (82). This arrangement allows the helices with only very slight deformation to undergo ''knobs into holes'' packing and to form stable dimerization surfaces (82). The Paircoil2 algorithm was created by analyzing a large set of known coiled-coil structures from the Protein Data Bank (74). The program's ability to identify coiled-coil structural motifs was then tested on a second set of known left-handed coiled-coils that was not included in the original set of structures (''leave-family-out cross validation''). A ''P-score'' for each amino acid is then calculated for each residue in the to be analyzed protein, which corresponds to the probability of that amino acid being found at a certain position within a heptad repeat. A P-score cutoff of 0.03 corresponds to >99% correct prediction of negative residues (specificity) and >73% correctly predicted positive residues (sensitivity) within a given sequence. The results of Paircoil2 analysis of the *b*- and *b*-like protein sequences are shown in Fig. 2. The *E. coli b* amino acid numbers are given in the *x* axis for reference, and the *P*-score for *E. coli b* is shown as a red line. The *P*-score of a *b*-homolog sequence from the cyanobacterium *Synechocystis* PCC 6803 is shown in blue. The horizontal black line depicts a *P*-score cutoff of 0.03.

With relatively few exceptions, all compared *b*-sequences have long stretches of amino acids that show *P*-scores of 0.03 or less. For *E. coli b*, the region between position 31 (closely following the ''hinge-proline'' at position 28) until 122 can be predicted with great confidence to consist of consecutive heptad repeats, which is strongly suggestive of a high propensity to form a left-handed coiled-coil structure. A different representation of the predicted heptad repeats shown in Fig. 2 was imaged with Jalview (81) and is given in Fig. 3. For better visualization, each of the heptad positions (*A, B, C, D, E, F, G*) was assigned a different shade of red from lightest (*A*) to darkest (*G*). A heptad pattern in Fig. 3 is very obvious and pronounced for all of the sequences. Some sequences show uninterrupted heptad repeats for more than 10 repeats. Some sequences show smaller numbers of uninterrupted repeats (e.g., *E. coli* subunit *b* shows six uninterrupted repeats) that are followed by discontinuities and then resume heptad repeat patterning.

Two types of discontinuities have been commonly observed in left-handed coiled-coil proteins (83). ''Stutters'' correspond to a three-residue deletion within a heptad and ''stammers'' correspond to four-residue deletions. These discontinuities in heptad repeats are well documented for classic left-handed coiled-coils and are discussed in Brown et al. (83). These authors hypothesized that the main function of the discontinuities is

TABLE 1 Species used for assessing the sequence similarity of *b*- or *b*-homologous proteins as shown in Fig. 1

001	*Streptococcus pyogenes* MGAS8232
002	*Leptospira borgpetersenii* serovar *Hardjo-bovis* JB197
003	*Escherichia coli*
004	*Pseudomonas entomophila* L48
005	*Candidatus Sulcia muelleri* str. Hc (*Homalodisca coagulata*)
006	*Pasteuria penetrans*
007	*Bacillus megaterium*
008	*Rhodobacter capsulatus*
009	*Lactococcus lactis* subsp. *lactis*
010	*Streptococcus mutans* UA159
011	*Acidithiobacillus ferrooxidans*
012	*Streptococcus sanguinis*
013	*Ruminococcus albus*
014	*Streptococcus bovis*
101	*Synechococcus* sp. PCC 6716
102	*Synechococcus elongatus* PCC 6301
103	*Synechococcus* sp. WH 5701
104	*Nostoc* sp. PCC 7120
105	*Anabaena variabilis* ATCC 29413
106	*Synechocystis* sp. PCC 6803
107	*Synechococcus* sp. JA-2-3B′a(2–13)
108	*Synechococcus* sp. WH 7805
109	*Synechococcus* sp. RS9917
110	*Synechococcus* sp. WH 8102
111	*Synechococcus* sp. CC9605
112	*Synechococcus* sp. CC9902
113	*Prochlorococcus marinus* str. MIT 9211
114	*Prochlorococcus marinus* str. MIT 9313
115	*Prochlorococcus marinus* subsp. *pastoris* str. CCMP1986
116	*Prochlorococcus marinus* str. MIT 9312
117	*Prochlorococcus marinus* str. NATL2A
118	*Thermosynechococcus elongatus* BP-1
119	*Synechococcus* sp. JA-3-3Ab
120	*Gloeobacter violaceus* PCC 7421
121	*Trichodesmium erythraeum* IMS101
122	*Crocosphaera watsonii* WH 8501
123	*Nostoc punctiforme* PCC 73102
124	*Prochlorococcus marinus* subsp. *marinus* str. CCMP1375
201	*Triticum aestivum*
202	*Spinacia oleracea*
203	*Pisum sativum*
204	*Arabidopsis thaliana*
205	*Zea mays*
206	*Nicotiana tabacum*
207	*Oenothera elata* subsp. *hookeri*
208	*Pelargonium x hortorum*
209	*Coffea arabica*
210	*Piper cenocladum*
211	*Drimys granadensis*
212	*Nuphar advena*
213	*Morus indica*
214	*Citrus sinensis*
215	*Gossypium hirsutum*

to accommodate different degrees of supercoiling within a coiled-coil structure. Stutters have been shown to produce an underwinding of the coils, whereas stammers seem to lead to overwinding of the helices. Importantly, depending on the position of a stutter within the heptad sequence, consecutive heptads with a stutter discontinuity might very easily be mistaken for undecad (7 + 4) repeats.

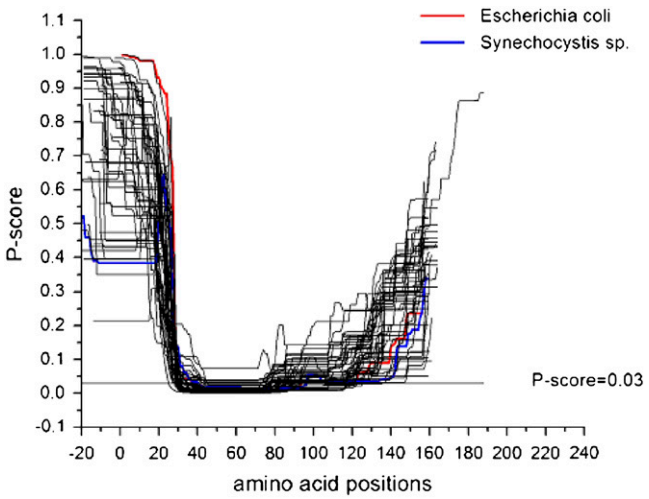

FIGURE 2 Structure prediction of the *b*-dimers. Paircoil2 (74) was used to determine the propensity of the *b*-sequences shown in Fig. 1 to be part of heptad sequences, a prerequisite for the formation of left-handed coiled-coil packing interactions. A *P*-score is given to each individual amino acid by the program that defines the probability of this amino acid to reside at a certain position within a heptad. A *P*-score lower than 0.03 (*black horizontal line*) indicates a very high probability of amino acids being at heptad positions. The red line indicates the *P*-scores for *E. coli* subunit *b*, and the blue line shows the *P*-scores for the *b*-subunit of the cyanobacterium *Synechocystis* sp. PCC 6803, which we also study in our lab group.

ESR spectroscopic determination of interspin and interchain distances within the *b*-dimer of *E. coli* ATP synthase

We utilized 38 single-cysteine mutations that were introduced into a soluble, truncated construct (31) of the *E. coli* *b*-dimer. In earlier work, we showed that the mutated and spin-labeled subunits *b*-dimerized normally under the conditions used for our ESR experiments (49). To determine interspin distances, ESR spectra of the soluble *b*-dimers were recorded in frozen solution at different salt concentrations and in the presence or absence of 20% (v/v) glycerol at either 193 K or 223 K. Although spectra acquired at 223 K showed more fine structure due to the higher mobility of the radicals, which increased our confidence in the subsequent simulations of these spectra according to Hustedt et al. (67), spectral simulation of the spectra acquired at 193 K revealed interspin distances that were within experimental error of those acquired at 223 K. Fig. 4 shows a representative set of ESR spectra of *b*-dimers that were MTS-SL at specific positions between amino acid 101 and 113 acquired at 193 K. The acquired spectra (*black*) are overlaid with the corresponding fitted curves (*red*). Fitting was accomplished as described in Hustedt et al. (67). Fig. 5 shows a typical set of ESR spectra of MTS-labeled *b*-dimers acquired at 223 K. The modified amino acids are given in the figure. In this figure as in the previous, the acquired spectra (*black*) are overlaid with the respective simulated spectra (*red*).

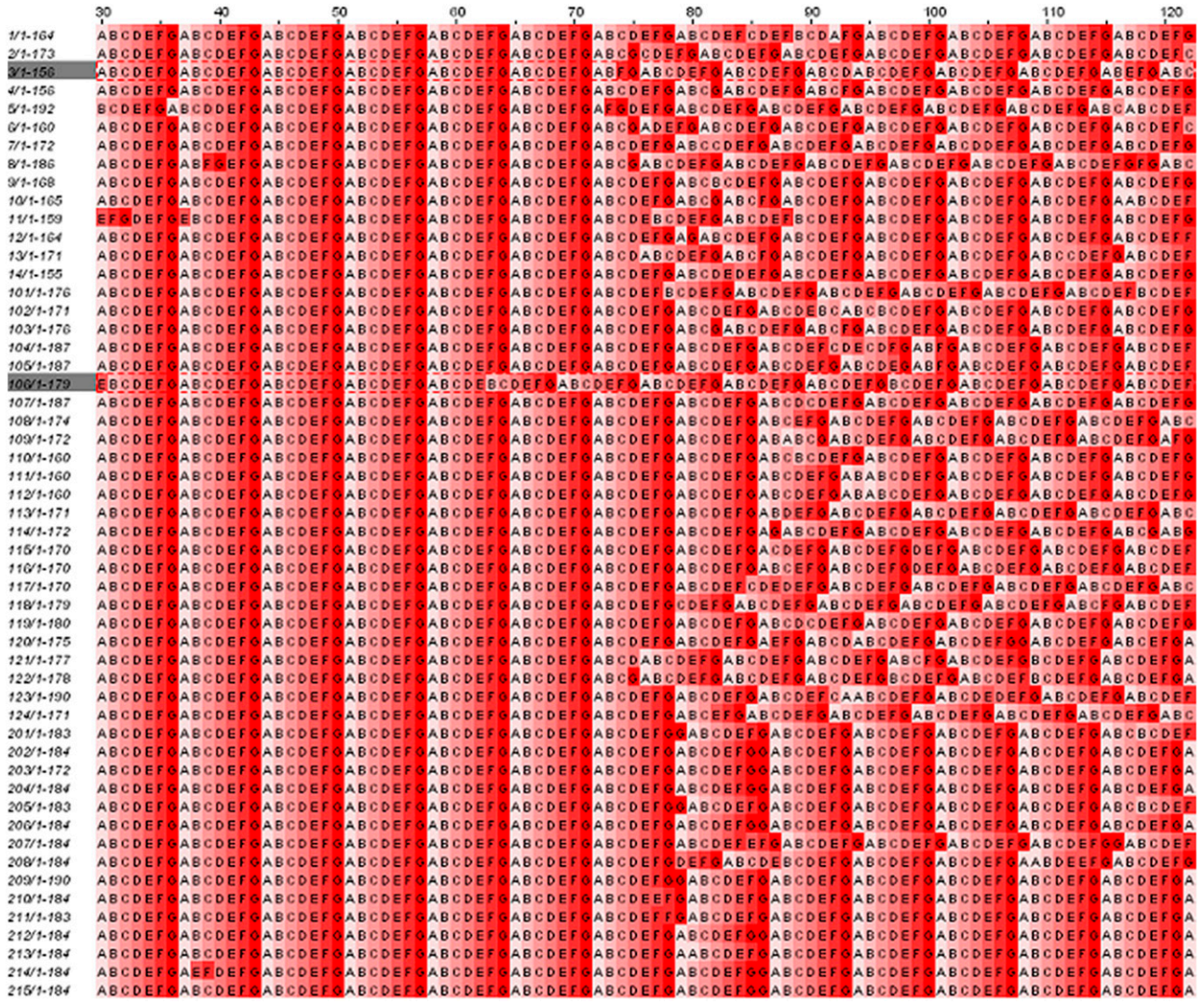

FIGURE 3 Heptad repeats are in all compared sequences. In a different visualization using Jalview version 2.2.1 (81), the Paircoil2-assigned heptad positions of the sequences compared in Fig. 1 are shown as different shades of red. The heptad positions for *E. coli* amino acids are shown in the third row. The amino acid numbers for *E. coli* are given on top of the figure. The alignment is shown between *E. coli* amino acids 30 and 122, which show the highest propensity for left-handed coiled-coil formation.

Molecular modeling of *E. coli* subunit *b* into left-handed coiled-coil structures

Using molecular modeling approaches as described (Wise and Vogel, preceding article) and briefly discussed in Materials and Methods, we were able to create low-energy structural models of the *E. coli* subunit *b*-dimer in an unstaggered left-handed coiled-coil. To test these structural models using ESR spectroscopy, we also parameterized the two spin labels used in this study, IAAT and MTS-SL, so that they could be incorporated into SA studies. Using these computational approaches, we were able to test whether the distances we measured in ESR experiments between MTS or IAAT spin labels introduced at various positions along the *b*-dimer could be accommodated by the models. We applied these approaches to two general strategies of modeling the spin-labeled mutated sequences.

First, we performed ab initio SA studies using distance and angle restraint tables for subunit *b* that we previously used to create acceptable dimeric models and included the ESR distances determined in a given set of experiments. We also tested whether the ESR measured distance could be satisfied by spin labels introduced into dimers that were constrained to the best dimeric models we had created previously for the underivatized subunit *b* proteins. In either case, the modeling was performed to determine whether the modeled left-handed coiled-coils could accommodate the distances we determined in our ESR measurements or whether these distances would be inconsistent with the models. The modeling of individually

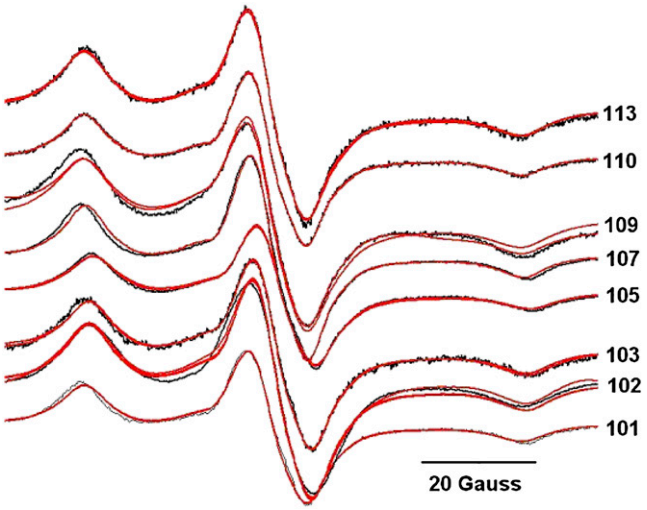

FIGURE 4 ESR spectra of MTS-SL site-specifically spin-labeled subunit *b* acquired at 193 K. A representative subset of ESR spectra in frozen solution of specifically spin-labeled subunits *b* is shown. The acquired spectra (shown in *black*) are overlaid by the spectra simulated (shown in *red*) according to Hustedt et al. (67) to obtain interspin distances. The spin-labeled amino acid positions are shown in the figure. χ^2 squared values of the fits (not shown) were between 9.5×10^2 and 1.7×10^4 for all fits. Control experiments performed at 223 K indicated that the distances derived from the spectra acquired at 193 K were within experimental error from those derived from spectra acquired at 223 K.

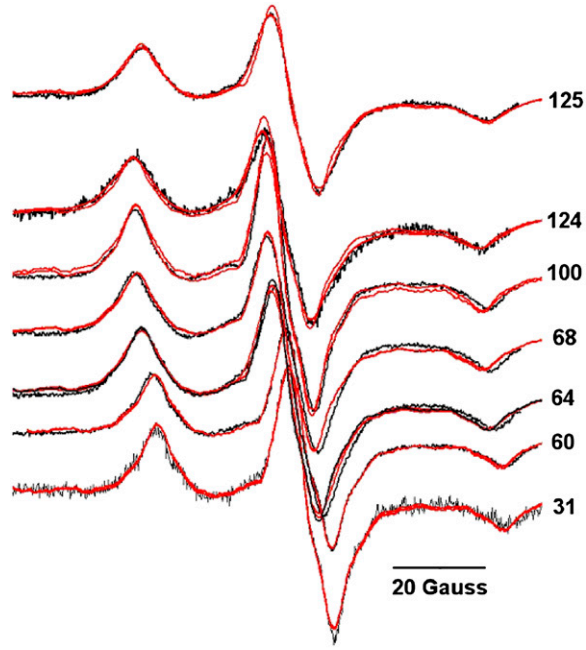

FIGURE 5 ESR spectra of MTS-SL site-specifically spin-labeled subunit *b* acquired at 223 K. A subset of ESR spectra in frozen solution of specifically spin-labeled subunits *b* is shown in black. The acquired spectra are overlaid by the spectra simulated according to Hustedt et al. (67) to obtain interspin distances (shown in *red*). The spin-labeled amino acid positions are given in the figure. χ^2 values of the fits were between 9.8×10^2 and 8×10^3 for all fits.

introduced spin-labeled residues allowed us to correlate average distances between doubly labeled proteins in collections of geometrically acceptable left-handed coiled-coil models with actual distance measurements made via ESR experimentation on doubly labeled subunit *b* proteins. In Fig. 6 are shown examples of lowest energy molecular models that were created as described above and that show MTS-cysteinyl amino acids at three randomly selected different positions (amino acid position 109, *left panel*; position 83, *middle panel*; and position 68, *right panel*) within the *b*-dimer in a left-handed coiled-coil structure. The interspin-label distances (NO to NO distances) derived from molecular modeling are shown in Fig. 6.

Interspin distances obtained by site-specific spin labeling correlate well with distances obtained from molecular modeling

Fig. 7 shows the comparison of interspin NO-NO distances obtained through evaluating the dipolar line broadening of spatially close spin labels attached to specific residues within the subunit *b*-dimer of *E. coli* F_0F_1-ATPase and the NO-NO distances obtained from molecular modeling based on left-handed nonstaggered coiled-coil models as shown in Fig. 3 in Wise and Vogel (preceding article). All structural models from which these results were obtained were solved with restraint data sets that produced dimeric left-handed coiled-coils that had no distance restraint violations >2 Å or dihedral restraint violations >5° and had no deviations from ideal bond lengths >0.1 Å and no deviations from ideal bond angles or impropers >5°. These acceptable models were all produced without violating the included ESR-derived restraint data, indicating that these left-handed coiled-coil

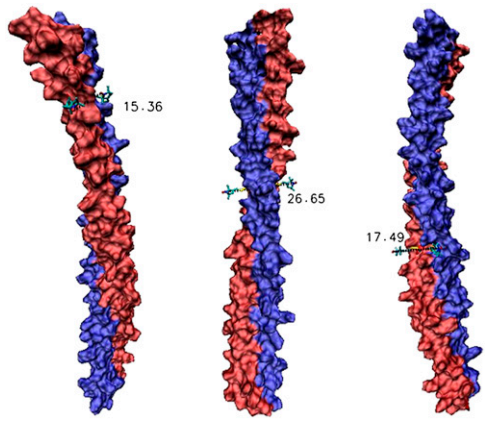

FIGURE 6 Molecular models of MTS-spin-labeled *E. coli* subunit *b*-dimers. Molecular models were obtained as described in Materials and Methods and in Wise and Vogel (preceding article). The lowest energy models obtained for MTS-labeled *b*-dimers are shown for amino acid positions 109, left panel, 83, middle panel, and 68, right panel. The interspin distances derived from the models are given in the figure. The dimers in the different panels were rotated relative to each other to better show the spin-labeled amino acid positions.

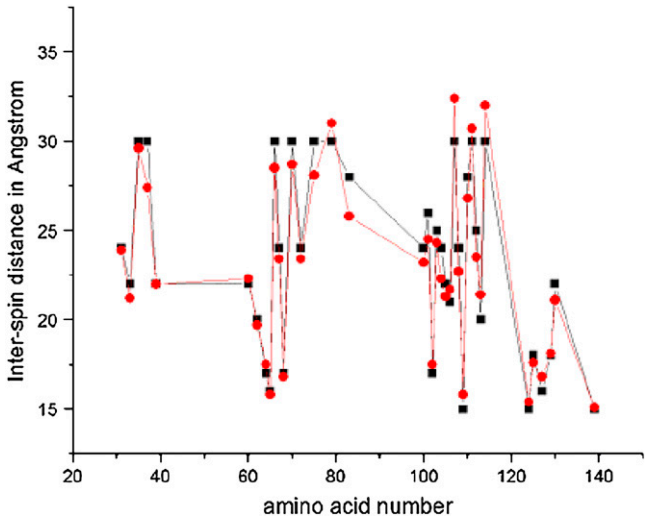

FIGURE 7 Comparison of distances from ESR experiments and molecular modeling. Interspin distances of MTS-SL-labeled *b*-dimers are compared that were either derived from the dipolar broadened ESR spectra (*squares*) or from molecular modeling the *E. coli* subunit *b*-dimer as a left-handed nonstaggered coiled-coil as described in Materials and Methods (*circles*) and see Fig. 3 of Wise and Vogel (preceding article). Distances stemming from ESR spectral simulations that were $\gg$25 Å were arbitrarily set to 30 Å. Distances up to 30 Å are given in the figure if they were reproducibly obtained from the simulations and if they also correlated well with the distances derived from molecular modeling.

models of the subunit *b*-dimer could accommodate the ESR-derived intersubunit distances. It should be noted that ESR distances determined by simulation to be much larger than 25 Å were arbitrarily set to 30 Å. Such distances cannot be accurately determined using the employed continuous wave ESR spectroscopy technique.

If simulations repeatedly gave distances between 25 and 30 Å in different experiments and if these distances also coincided with the distances obtained by molecular modeling, their values were included as measured into the figure. The χ^2 values of the fits were between 9.5×10^2 and 1.7×10^4 for all fits. The χ^2 values differed depending on the protein concentrations and the resulting variations in the signal/noise ratios of the spectra. The squares designate the ESR-derived interspin distances, the circles correspond to the distances calculated from molecular modeling, as described in Materials and Methods. The correlation between experimentally determined and modeled distances is striking and very strongly suggests that indeed the *E. coli b*-dimer can fold as a left-handed coiled-coil structure under the conditions used in these experiments.

Initial attempts at including ESR-derived distance restraints into SA experiments to generate models of right-handed coiled-coils have been unsuccessful mostly because of the lack of predictably and reproducibly in obtaining right-handed coiled-coil structures (see Wise and Vogel, preceding article). This may be due to the fact that the right-handed coiled-coil restraints used were based on data derived from manipulated tetrameric right-handed coiled-coil structures (Wise and Vogel, preceding article) and may not be sufficiently complete to guarantee right-handed dimeric structures from SA experiments. Additionally, it should be noted that only a short portion of the subunit *b*-structure could be modeled as a right-handed coiled-coil, whereas we were unable to obtain such a structure for the full-length cytosolic part of b_2. These problems made unequivocal distinction between right-handed and left-handed coiled-coil structures by simply comparing putative differences in the interspin distances for the two different structures not yet possible.

DISCUSSION

The structure of the subunit *b*-dimer of bacterial F_0F_1-ATP synthases and its role as a stator during rotational catalysis remains one of the last unsolved questions in the elucidation of the mechanism of this fascinating enzyme. The rotational mechanism as we understand it involves the proton-driven rotation of 10–15 subunits *c* (depending on the source of the ATP synthase), which is then coupled to the three-step rotary motion of the central-stalk subunits γ and ε, which can each be subdivided into two unequal substeps (for recent advances see Adachi et al. (84)). Despite tremendous efforts, relatively little is known about the structure of the bacterial external stalk. So far no high-resolution structure is available for the *b*-dimer itself. Most information to date for the cytosolic portion of *b* stems from circular dichroism spectroscopy, disulfide cross-linking studies, ESR spectroscopy, and the x-ray structural model of a monomer of the dimerization domain of the *E. coli* F_0 *b*-subunit.

Although the curved structure shown in the x-ray crystallographic model of mitochondrial subunit *b* together with its helper proteins *d* and *F6* suggests that this protein complex may be more or less rigid and inflexible in nature (43,44), studies of the homologous bacterial subunit *b*-dimer strongly implied a rather flexible character of the proteins with a high degree of plasticity. As discussed earlier, sequence insertions and deletions as well as substitutions with peptide sequences from different *b*-proteins still allowed the assembly of functional ATP synthase (37–41). Whether a flexible connection between F_1 and F_0 is needed for interim storage of energy during rotation of the subunit-*c* ring until enough energy is accumulated for the larger rotary steps of subunit γ as was suggested by the Junge lab (13,14) and others, or whether the second, external stalk functions as a rigid stator to simply facilitate F_0F_1-assembly and stabilize the structure has yet to be elucidated. Alternatively, although rather unlikely, one could hypothesize that bacterial and chloroplast ATP synthases, which both contain dimeric external stalks, might function differently from those enzyme complexes found in mitochondria. In any case, understanding the structure and potential dynamics of the *b*-dimer will have an immense

impact on our understanding of the rotary mechanism of nature's smallest and most efficient rotary motor.

Alignment and secondary structure prediction of various bacterial, cyanobacterial, and plant subunits *b*

Of the 53 different *b* and *b*-homologous proteins that were aligned in Fig. 1, only limited sequence similarity could be identified. This finding seems to be consistent with a structural role of the *b*-dimer that does not require specific interactions of catalytically important amino acids with the rest of the complex. The fact that indeed these different amino acid sequences may adopt very similar overall structures became obvious when the amino acids were compared with regard to their propensity to form certain structural assemblies. Using the improved structure prediction program Paircoil2 (74), the *b*-sequences were examined with regard to their potential to form a left-handed coiled-coil structure that is observed in many parallel, extended α-helical proteins. The Paircoil2 algorithm assigns each amino acid a score that indicates its probability of contributing to heptad repeats that are characteristic of left-handed coiled-coil structures. The *P*-score of $\sim$0.03 for *E. coli b*-subunit residues 31 to $\sim$124 implies a very high (>97%) probability that the corresponding amino acids are part of a heptad repeat sequences. Figs. 2 and 3 show that the amino acid sequences for *b*-subunits from very different organisms also have extended heptad repeat stretches in their sequence. Some of the predicted repeats stretch for 100 amino acids or more and at *P*-scores of 0.03–0.045. For the *E. coli b*-dimer this corresponds to $\sim$60% of the total *b*-protein length or 70% of the cytosolic part of *b*. These observations strongly suggest that the *b*-proteins analyzed here seem capable of forming left-handed coiled-coil structural interactions.

At first glance, some of the repeats seem to be broken by 3 or 4 amino acid inserts or deletions (stutters or stammers). These sequences then resume the heptad repeat successions. Such discontinuities have been reported as an integral part of many left-handed coiled-coils and were found to cause under- or overwinding of the helical supertwist (83) as well as allow formation of interaction interfaces that might stabilize the helical packing. It is interesting to note that the stutters observed in the *E. coli b* occur at amino acids 73/74 and then again at 93/94, an area that we proposed earlier to be in direct contact with soluble ATPase (49). The existence of stutters in this particular part of subunit *b* may be to create a proper interaction surface for binding to the F_1-ATPase. In summary, it seems clear from Figs. 2 and 3 that extended series of heptad repeats, sometimes interrupted by stammers or stutters, are to be found in the *b*-sequences analyzed. These results strongly suggest that left-handed coiled-coil structures can be accommodated in *b*-subunits from many different species.

Molecular modeling of *E. coli* subunit *b*-dimer as a left-handed coiled-coil structure and validation of the model using site-directed spin labeling and ESR spectroscopy

The conserved heptad repeat sequences found for almost all *b*-subunit analyses encouraged us to create models of the soluble part of *E. coli* subunit *b* using molecular modeling techniques as described in Wise and Vogel (preceding article). The models created using SA techniques showed that subunit *b*-dimer can exist as low-energy left-handed coiled-coil structures that have no violations in protein geometry, bond lengths, or ϕ or ψ dihedral angles. The lowest energy structure was then used for validation by ESR spectroscopy. To achieve this goal, 38 single cysteine mutations were generated in an otherwise cysteineless protein background of a soluble part of *E. coli b* that was first introduced by the Dunn lab (31). Since the *b*-subunits are coded by a single gene, this approach resulted in *b*-dimers that carry the mutation at the same amino acid position in each of the monomers. Modification of the introduced cysteines with cysteine-specific spin labels and ESR spectroscopy of samples in frozen solution then allowed us to determine the distances between the two introduced radicals by evaluating the line broadening of the resulting ESR spectra caused by dipolar interaction of the spins. ESR spectra were recorded either at 193 K or at 223 K and representative sets of ESR spectra overlaid with the corresponding simulated curves for distance estimation are shown in Figs. 4 and 5. Although acquisition of the spectra at 223 K allowed more spectral detail, the distances we obtained through spectral simulation were within error range whether the spectra were obtained at 223 or 193 K. The spectra shown are those of MTS-spin-labeled subunit *b*-dimers. The use of the somewhat longer and less rotationally restricted acetamido-TEMPO spin label resulted in large variations in estimated distances and was deemed to not be very reliable.

To compare the interspin distances obtained from ESR experiments with the distances we obtained from molecular modeling of the subunit *b*-dimer, we created the topology and parameter files for both spin labels used in our experiments, IAAT and MTS-SL, and introduced the corresponding cysteinyl spin label moieties into the molecular modeling protocols together with distance restraints for interspin distances that were obtained from individual ESR experiments. We then produced left-handed coiled-coil models for each IAAT- or MTS-SL-substituted subunit *b*-dimer and determined whether the resultant models could accommodate the ESR distances without violating the left-handed coiled-coil structures. Results from these modeling experiments (examples are shown in Fig. 6) showed that distances between modeled spin labels in these low-energy left-handed coiled-coil structures correlated very well with the distances we calculated from cysteinyl-spin-labeled *b*-dimers in the ESR experiments (see Fig. 7). At no position tested did the modeling of left-handed

coiled-coil dimers conflict with an included ESR-derived distance restraint.

It should be mentioned here that some of the interspin distances in the *b*-dimer, especially those on the outer surfaces of the helices, were too large to be accurately determined by the continuous wave ESR spectroscopy that we performed. We arbitrarily set these longer distances to be 30 Å in the modeling experiments shown in Fig. 7. What is remarkable in Fig. 7 is the exceptional correlation of the short, more accurately determined interspin distances as well as the overall overlay of the distance variations along the amino acid sequence.

It has recently been proposed that the *E. coli* subunit *b*-dimer folds as a very unusual right-handed coiled-coil (34,35). The reasons that the authors gave for this so far not observed dimer packing interaction were their observation of what they considered a ''slight right-handed twist'' of a putative dimerization surface in the x-ray structural model of a monomeric form of the *b*-dimerization domain as well as ''out-of-phase'' disulfide cross-links in the amino acid range from position 68 to 93. We have observed unstaggered cross-links at positions 101, 105, and 109 (data not shown), as others have (for review see Altendorf et al. (85)) at regions below and above those residue pairs reported by Del Rizzo et al. (35) to form staggered disulfide cross-links. These results taken together create problems in rationalizing the overall fold of subunit *b*, since exceptionally rapid changes from unstaggered to staggered to unstaggered coiled-coils need to be accommodated. Curiously, the sequence that seems to allow the formation of the ''staggered'' cross-links is very close to the observed stutters in the heptad repeats as identified in Figs. 2 and 3. Due to the lack of a stringent model for a right-handed coiled-coil (discussed in Wise and Vogel, preceding article) and also due to the short stretch of subunit *b* that seems to show this unusual behavior of staggered cross-links (only 25 residues), we were unable to determine whether the distance data derived from ESR spectroscopy could distinguish between a right-handed, staggered arrangement and the left-handed coiled-coil that is supported by our modeling.

Assuming that a left-handed coiled-coil arrangement with a loosening of the packing due to the stutters predicted for this region (see Wise and Vogel, preceding article, and Brown et al. (83)) exists for the subunit *b*-dimer, one can speculate that the formation of an ''unstaggered'' dimer interaction surface may position the thiol groups in geometries that are unfavorable for chemical cross-links, whereas amino acids four to seven residues away may turn into the helical interfaces (maybe more so due to the stutters) and approach a more favorable reaction geometry. This would have the effect that in the course of the 24-h disulfide-formation incubations as described in Del Rizzo et al. (35) cross-links might form between staggered positions that would normally not have been favored. In any case, interpretation of these experiments that show only a short sequence of subunit *b* to be ''out of phase'' remains problematic.

CONCLUSIONS

Using ESR spectroscopy and site-directed spin labeling of 38 individual residues in subunit *b*, we were able to generate a set of intermolecular distances between defined points in the dimer. We employed structure prediction programs that strongly suggested that the subunit *b*-dimer can adopt left-handed coiled-coil structures. Molecular modeling of the *E. coli* subunit *b*-dimer in ab initio SA experiments that used restraints based on ideal left-handed coiled-coil proteins allowed us to identify acceptable left-handed coiled-coil structures for the soluble portion of the *E. coli b*-dimer. Incorporation of the ESR-derived distance data into these models allowed us to validate the sequence-based predicted heptad repeat patterns and the left-handed coiled-coil structural models derived from the SA modeling experiments. The results indicate that the subunit *b*-dimer of the *E. coli* ATP synthase can adopt a left-handed coiled-coil structure between residues 31 and 116. Due to the lack of reproducibility of right-handed coiled-coil structural models for b_2 as well as the fact that only a short portion of the *b*-dimer could be modeled in the form of a right-handed coiled-coil, we are not yet able to unambiguously distinguish between the two potential different structures by comparing interspin distances.

Although the question of a putative elastic nature of the subunit *b*-dimer could not be addressed in this approach, these described experiments have set the stage for experiments currently underway in our lab, where we will test potential structural deviations of the *b*-dimer upon binding to F_1. We are also in the course of investigating potential changes in the *b*-dimer packing in the whole F_0F_1-ATP synthase during nucleotide binding and formation of ATP-hydrolysis transition states to test whether catalytic turnover causes structural transitions in the *b*-dimer. These latter experiments seem the perfect means to study the potential elastic nature of the *b*-dimer in the course of catalytic turnover.

The authors thank Stanley D. Dunn, Canada, for providing the plasmid coding for the (cysteineless) truncated subunit *b*, pDM3, as well as several of the plasmids used to express single cysteine mutants in subunit *b* and for performing some of the cross-link studies. The authors also appreciate the gift of MTS-spin label from Kalman Hideg, Hungary. Special thanks go to Eric J. Hustedt, Vanderbilt University, Nashville, for providing us with the program PAKERICH and his invaluable help in getting us started with ESR distance simulations. We also thank Markus Dittrich (University of Illinois at Urbana-Champaign) for initial help with the spin label QM calculations.

This work was funded by a grant from the National Science Foundation (MCB 0415713) to P.D.V.

REFERENCES

1. Boyer, P. D. 1997. The ATP synthase—a splendid molecular machine. *Annu. Rev. Biochem.* 66:717–749.
2. Senior, A. E., S. Nadanaciva, and J. Weber. 2002. The molecular mechanism of ATP synthesis by F1F0-ATP synthase. *Biochim. Biophys. Acta.* 1553:188–211.
3. Yoshida, M., E. Muneyuki, and T. Hisabori. 2001. ATP synthase—a marvellous rotary engine of the cell. *Nat. Rev. Mol. Cell Biol.* 2:669–677.

4. Rodgers, A. J., S. Wilkens, R. Aggeler, M. B. Morris, S. M. Howitt, and R. A. Capaldi. 1997. The subunit delta-subunit *b* domain of the *Escherichia coli* F1F0 ATPase. The *b* subunits interact with F1 as a dimer and through the delta subunit. *J. Biol. Chem.* 272:31058–31064.
5. Dunn, S. D., and J. Chandler. 1998. Characterization of a b2delta complex from *Escherichia coli* ATP synthase. *J. Biol. Chem.* 273: 8646–8651.
6. Ogilvie, I., S. Wilkens, A. J. Rodgers, R. Aggeler, and R. A. Capaldi. 1998. The second stalk: the delta-b subunit connection in ECF1F0. *Acta Physiol. Scand. Suppl.* 643:169–175.
7. Wilkens, S., and R. A. Capaldi. 1998. ATP synthase's second stalk comes into focus. *Nature.* 393:29.
8. Stalz, W., J. Greie, G. Deckers-Hebestreit, and K. Altendorf. 2003. Direct interaction of subunits a and b of the F0 complex of *Escherichia coli* ATP synthase by forming an ab2 subcomplex. *J. Biol. Chem.* 278:27068–27071.
9. Vik, S. B., J. C. Long, T. Wada, and D. Zhang. 2000. A model for the structure of subunit a of the *Escherichia coli* ATP synthase and its role in proton translocation. *Biochim. Biophys. Acta.* 1458:457–466.
10. Angevine, C. M., and R. H. Fillingame. 2003. Aqueous access channels in subunit a of rotary ATP synthase. *J. Biol. Chem.* 278:6066–6074.
11. Zhang, D., and S. B. Vik. 2003. Close proximity of a cytoplasmic loop of subunit a with c subunits of the ATP synthase from *Escherichia coli*. *J. Biol. Chem.* 278:12319–12324.
12. Greie, J., T. Heitkamp, and K. Altendorf. 2004. The transmembrane domain of subunit *b* of the *Escherichia coli* F_1F_0 ATP synthase is sufficient for H^+-translocating activity together with subunits a and c. *Eur. J. Biochem.* 271:3036–3042.
13. Cherepanov, D. A., A. Y. Mulkidjanian, and W. Junge. 1999. Transient accumulation of elastic energy in proton translocating ATP synthase. *FEBS Lett.* 449:1–6.
14. Junge, W. 1999. ATP synthase and other motor proteins. *Proc. Natl. Acad. Sci. USA.* 96:4735–4737.
15. Abrahams, J. P., A. G. Leslie, R. Lutter, and J. E. Walker. 1994. Structure at 2.8 Å resolution of F1-ATPase from bovine heart mitochondria. *Nature.* 370:621–628.
16. Bowler, M. W., M. G. Montgomery, A. G. W. Leslie, and J. E. Walker. 2006. How azide inhibits ATP hydrolysis by the F-ATPases. *Proc. Natl. Acad. Sci. USA.* 103:8646–8649.
17. Cabezón, E., M. G. Montgomery, A. G. W. Leslie, and J. E. Walker. 2003. The structure of bovine F1-ATPase in complex with its regulatory protein IF1. *Nat. Struct. Biol.* 10:744–750.
18. Shirakihara, Y., A. G. Leslie, J. P. Abrahams, J. E. Walker, T. Ueda, Y. Sekimoto, M. Kambara, K. Saika, Y. Kagawa, and M. Yoshida. 1997. The crystal structure of the nucleotide-free alpha 3 beta 3 subcomplex of F1-ATPase from the thermophilic Bacillus PS3 is a symmetric trimer. *Structure.* 5:825–836.
19. Bianchet, M. A., J. Hullihen, P. L. Pedersen, and L. M. Amzel. 1998. The 2.8-Å structure of rat liver F1-ATPase: configuration of a critical intermediate in ATP synthesis/hydrolysis. *Proc. Natl. Acad. Sci. USA.* 95:11065–11070.
20. Stock, D., A. G. Leslie, and J. E. Walker. 1999. Molecular architecture of the rotary motor in ATP synthase. *Science.* 286:1700–1705.
21. Wilkens, S., F. W. Dahlquist, L. P. McIntosh, L. W. Donaldson, and R. A. Capaldi. 1995. Structural features of the epsilon subunit of the *Escherichia coli* ATP synthase determined by NMR spectroscopy. *Nat. Struct. Biol.* 2:961–967.
22. Wilkens, S., S. D. Dunn, J. Chandler, F. W. Dahlquist, and R. A. Capaldi. 1997. Solution structure of the N-terminal domain of the delta subunit of the *E. coli* ATP synthase. *Nat. Struct. Biol.* 4:198–201.
23. Uhlin, U., G. B. Cox, and J. M. Guss. 1997. Crystal structure of the epsilon subunit of the proton-translocating ATP synthase from *Escherichia coli*. *Structure.* 5:1219–1230.
24. Zhang, D., and S. B. Vik. 2003. Helix packing in subunit a of the *Escherichia coli* ATP synthase as determined by chemical labeling and proteolysis of the cysteine-substituted protein. *Biochemistry.* 42: 331–337.
25. Walker, J. E., M. Saraste, and N. J. Gay. 1984. The unc operon. Nucleotide sequence, regulation and structure of ATP-synthase. *Biochim. Biophys. Acta.* 768:164–200.
26. Dunn, S. D. 1992. The polar domain of the *b* subunit of *Escherichia coli* F1F0-ATPase forms an elongated dimer that interacts with the F1 sector. *J. Biol. Chem.* 267:7630–7636.
27. Revington, M., D. T. McLachlin, G. S. Shaw, and S. D. Dunn. 1999. The dimerization domain of the *b* subunit of the *Escherichia coli* F_1F_0-ATPase. *J. Biol. Chem.* 274:31094–31101.
28. Revington, M., S. D. Dunn, and G. S. Shaw. 2002. Folding and stability of the *b* subunit of the F_1F_0 ATP synthase. *Protein Sci.* 11: 1227–1238.
29. Greie, J. C., G. Deckers-Hebestreit, and K. Altendorf. 2000. Secondary structure composition of reconstituted subunit *b* of the *Escherichia coli* ATP synthase. *Eur. J. Biochem.* 267:3040–3048.
30. Dmitriev, O., P. C. Jones, W. Jiang, and R. H. Fillingame. 1999. Structure of the membrane domain of subunit *b* of the *Escherichia coli* F_0F_1 ATP synthase. *J. Biol. Chem.* 274:15598–15604.
31. McLachlin, D. T., and S. D. Dunn. 1997. Dimerization interactions of the *b* subunit of the *Escherichia coli* F1F0-ATPase. *J. Biol. Chem.* 272:21233–21239.
32. Dunn, S. D., D. T. McLachlin, and M. Revington. 2000. The second stalk of *Escherichia coli* ATP synthase. *Biochim. Biophys. Acta.* 1458: 356–363.
33. Dunn, S. D., M. Revington, D. J. Cipriano, and B. H. Shilton. 2000. The *b* subunit of *Escherichia coli* ATP synthase. *J. Bioenerg. Biomembr.* 32:347–355.
34. Del Rizzo, P. A., Y. Bi, S. D. Dunn, and B. H. Shilton. 2002. The ''second stalk'' of *Escherichia coli* ATP synthase: structure of the isolated dimerization domain. *Biochemistry.* 41:6875–6884.
35. Del Rizzo, P. A., Y. Bi, and S. D. Dunn. 2006. ATP synthase *b* subunit dimerization domain: a right-handed coiled coil with offset helices. *J. Mol. Biol.* 364:735–746.
36. Steigmiller, S., M. Börsch, P. Gräber, and M. Huber. 2005. Distances between the *b*-subunits in the tether domain of F0F1-ATP synthase from *E. coli*. *Biochim. Biophys. Acta.* 1708:143–153.
37. Sorgen, P. L., T. L. Caviston, R. C. Perry, and B. D. Cain. 1998. Deletions in the second stalk of F1F0-ATP synthase in *Escherichia coli*. *J. Biol. Chem.* 273:27873–27878.
38. Sorgen, P. L., M. R. Bubb, and B. D. Cain. 1999. Lengthening the second stalk of F_1F_0 ATP synthase in *Escherichia coli*. *J. Biol. Chem.* 274:36261–36266.
39. Grabar, T. B., and B. D. Cain. 2003. Integration of *b* subunits of unequal lengths into F1F0-ATP synthase. *J. Biol. Chem.* 278:34751–34756.
40. Grabar, T. B., and B. D. Cain. 2004. Genetic complementation between mutant *b* subunits in F1F0 ATP synthase. *J. Biol. Chem.* 279:31205–31211.
41. Bhatt, D., S. P. Cole, T. B. Grabar, S. B. Claggett, and B. D. Cain. 2005. Manipulating the length of the *b* subunit F1 binding domain in F1F0 ATP synthase from *Escherichia coli*. *J. Bioenerg. Biomembr.* 37:67–74.
42. Claggett, S. B., T. B. Grabar, S. D. Dunn, and B. D. Cain. 2007. Functional incorporation of chimeric *b* subunits into F1F0 ATP synthase. *J. Bacteriol.* 189:5463–5471.
43. Dickson, V. K., J. A. Silvester, I. M. Fearnley, A. G. W. Leslie, and J. E. Walker. 2006. On the structure of the stator of the mitochondrial ATP synthase. *EMBO J.* 25:2911–2918.
44. Walker, J. E., and V. K. Dickson. 2006. The peripheral stalk of the mitochondrial ATP synthase. *Biochim. Biophys. Acta.* 1757:286–296.
45. Weber, J. 2006. ATP synthase: subunit-subunit interactions in the stator stalk. *Biochim. Biophys. Acta.* 1757:1162–1170.
46. Weber, J. 2007. ATP synthase—the structure of the stator stalk. *Trends Biochem. Sci.* 32:53–56.

47. Weber, J., S. Wilke-Mounts, and A. E. Senior. 2003. Identification of the F1-binding surface on the delta-subunit of ATP synthase. *J. Biol. Chem.* 278:13409–13416.

48. Kersten, M. V., S. D. Dunn, J. G. Wise, and P. D. Vogel. 2000. Site-directed spin-labeling of the catalytic sites yields insight into structural changes within the F0F1-ATP synthase of *Escherichia coli*. *Biochemistry*. 39:3856–3860.

49. Motz, C., T. Hornung, M. Kersten, D. T. McLachlin, S. D. Dunn, J. G. Wise, and P. D. Vogel. 2004. The subunit *b* dimer of the F0F1-ATP synthase: interaction with F1-ATPase as deduced by site-specific spin-labeling. *J. Biol. Chem.* 279:49074–49081.

50. Vogel-Claude, P., G. Schäfer, and W. E. Trommer. 1988. Synthesis of a photoaffinity-spin-labeled derivative of ATP and its first application to F1-ATPase. *FEBS Lett.* 227:107–109.

51. Vogel, P. D., J. H. Nett, H. E. Sauer, K. Schmadel, R. L. Cross, and W. E. Trommer. 1992. Nucleotide binding sites on mitochondrial F1-ATPase. Electron spin resonance spectroscopy and photolabeling by azido-spin-labeled adenine nucleotides support an adenylate kinase-like orientation. *J. Biol. Chem.* 267:11982–11986.

52. Burgard, S., J. H. Nett, H. E. Sauer, Y. Kagawa, H. J. Schäfer, J. G. Wise, P. D. Vogel, and W. E. Trommer. 1994. Effects of magnesium ions on the relative conformation of nucleotide binding sites of F1-ATPases as studied by electron spin resonance spectroscopy. *J. Biol. Chem.* 269:17815–17819.

53. Lösel, R. M., A. H. Erbes, J. H. Nett, J. G. Wise, G. Berger, G. Girault, and P. D. Vogel. 1996. Asymmetry of catalytic but not of noncatalytic sites on *Escherichia coli* F1-ATPase in solution as observed using electron spin resonance spectroscopy. *Spectrochimica Acta. Part A.* 52:73–83.

54. Neuhofen, S., H. Theyssen, J. Reinstein, W. E. Trommer, and P. D. Vogel. 1996. Nucleotide binding to the heat-shock protein DnaK as studied by ESR spectroscopy. *Eur. J. Biochem.* 240:78–82.

55. Lösel, R. M., J. G. Wise, and P. D. Vogel. 1997. Asymmetry of catalytic but not of noncatalytic sites on *Escherichia coli* F1-ATPase in solution as observed using electron spin resonance spectroscopy. *Biochemistry.* 36:1188–1193.

56. Scheibel, T., S. Neuhofen, T. Weikl, C. Mayr, J. Reinstein, P. D. Vogel, and J. Buchner. 1997. ATP-binding properties of human Hsp90. *J. Biol. Chem.* 272:18608–18613.

57. Haller, M., U. Hoffmann, T. Schanding, R. S. Goody, and P. D. Vogel. 1997. Nucleotide hydrolysis-dependent conformational changes in p21(ras) as studied using ESR spectroscopy. *J. Biol. Chem.* 272: 30103–30107.

58. Burgard, S., M. Harada, Y. Kagawa, W. E. Trommer, and P. D. Vogel. 2003. Association of alpha-subunits with nucleotide-modified beta-subunits induces asymmetry in the catalytic sites of the F1-ATPase alpha3beta3-hexamer. *Cell Biochem. Biophys.* 39:175–181.

59. Delannoy, S., I. L. Urbatsch, G. Tombline, A. E. Senior, and P. D. Vogel. 2005. Nucleotide binding to the multidrug resistance P-glycoprotein as studied by ESR spectroscopy. *Biochemistry.* 44: 14010–14019.

60. Dias, J. M., C. Szegedi, I. Jóna, and P. D. Vogel. 2006. Insights into the regulation of the ryanodine receptor: differential effects of Mg2+ and Ca2+ on ATP binding. *Biochemistry.* 45:9408–9415.

61. Trommer, W. E., and P. D. Vogel. 1992. Photoaffinity spin labeling. *In*: Bioactive Spin Labels. R. Zhdanov, editor. Springer, Berlin, Germany. 405–427.

62. Vogel, P. D. 2000. Insights into ATP synthase structure and function using affinity and site-specific spin labeling. *J. Bioenerg. Biomembr.* 32:413–421.

63. Panse, V. G., P. Vogel, W. E. Trommer, and R. Varadarajan. 2000. A thermodynamic coupling mechanism for the disaggregation of a model peptide substrate by chaperone secB. *J. Biol. Chem.* 275:18698–18703.

64. Panse, V. G., K. Beena, R. Philipp, W. E. Trommer, P. D. Vogel, and R. Varadarajan. 2001. Electron spin resonance and fluorescence studies of the bound-state conformation of a model protein substrate to the chaperone SecB. *J. Biol. Chem.* 276:33681–33688.

65. Bradford, M. M. 1976. A rapid and sensitive method for the quantitation of microgram quantities of protein utilizing the principle of protein-dye binding. *Anal. Biochem.* 72:248–254.

66. Laemmli, U. K. 1970. Cleavage of structural proteins during the assembly of the head of bacteriophage T4. *Nature.* 227:680–685.

67. Hustedt, E. J., R. A. Stein, L. Sethaphong, S. Brandon, Z. Zhou, and S. C. Desensi. 2006. Dipolar coupling between nitroxide spin labels: the development and application of a tether-in-a-cone model. *Biophys. J.* 90:340–356.

68. Rabenstein, M. D., and Y. K. Shin. 1995. Determination of the distance between two spin labels attached to a macromolecule. *Proc. Natl. Acad. Sci. USA.* 92:8239–8243.

69. Steinhoff, H. J., N. Radzwill, W. Thevis, V. Lenz, D. Brandenburg, A. Antson, G. Dodson, and A. Wollmer. 1997. Determination of interspin distances between spin labels attached to insulin: comparison of electron paramagnetic resonance data with the x-ray structure. *Biophys. J.* 73:3287–3298.

70. Schmidt, M. W., K. K. Baldridge, J. A. Boatz, S. T. Elbert, M. S. Gordon, J. H. Jensen, S. Koseki, N. Matsunaga, K. A. Nguyen, S. Su, T. L. Windus, M. Dupuis, and J. A. Montgomery. 1993. General atomic and molecular electronic structure system. *J. Comput. Chem.* 14:1347–1363.

71. Schaftenaar, G., and J. H. Noordik. 2000. The effect of isodensity surface sampling on ESP derived charges and the effect of adding bondcenters on DMA derived charges. *J. Comput. Aided Mol. Des.* 14:233–242.

72. Sale, K., C. Sár, K. A. Sharp, K. Hideg, and P. G. Fajer. 2002. Structural determination of spin label immobilization and orientation: a Monte Carlo minimization approach. *J. Magn. Reson.* 156:104–112.

73. Sanner, M. F., A. J. Olson, and J. C. Spehner. 1996. Reduced surface: an efficient way to compute molecular surfaces. *Biopolymers.* 38:305–320.

74. McDonnell, A. V., T. Jiang, A. E. Keating, and B. Berger. 2006. Paircoil2: improved prediction of coiled coils from sequence. *Bioinformatics.* 22:356–358.

75. Wolf, E., P. S. Kim, and B. Berger. 1997. MultiCoil: a program for predicting two- and three-stranded coiled coils. *Protein Sci.* 6:1179–1189.

76 Humphrey, W., A. Dalke and K. Schulten. 1996. VMD: visual molecular dynamics. *J. Mol. Graph.* 14:33–38, 27–28.

77. Ousterhout, J. C. 1994. Tcl and the Tk Toolkit. Addison-Wesley Professional, Upper Saddle River, NJ.

78. Sanner, M. F. 1999. Python: a programming language for software integration and development. *J. Mol. Graph. Model.* 17:57–61.

79. Schwieters, C. D., J. J. Kuszewski, N. Tjandra, and G. M. Clore. 2003. The Xplor-NIH NMR molecular structure determination package. *J. Magn. Reson.* 160:65–73.

80. Chenna, R., H. Sugawara, T. Koike, R. Lopez, T. J. Gibson, D. G. Higgins, and J. D. Thompson. 2003. Multiple sequence alignment with the Clustal series of programs. *Nucleic Acids Res.* 31:3497–3500.

81. Clamp, M., J. Cuff, S. M. Searle, and G. J. Barton. 2004. The Jalview Java alignment editor. *Bioinformatics.* 20:426–427.

82. Crick, F. H. C. 1953. The packing of alpha-helices: simple coiled-coils. *Acta Crystallogr.* 6:689–697.

83. Brown, J. H., C. Cohen, and D. A. Parry. 1996. Heptad breaks in alpha-helical coiled coils: stutters and stammers. *Proteins.* 26:134–145.

84. Adachi, K., K. Oiwa, T. Nishizaka, S. Furuike, H. Noji, H. Itoh, M. Yoshida, and K. J. Kinosita. 2007. Coupling of rotation and catalysis in F_1-ATPase revealed by single-molecule imaging and manipulation. *Cell.* 130:309–321.

85. Altendorf, K., W. Stalz, J. Greie, and G. Deckers-Hebestreit. 2000. Structure and function of the F_0 complex of the ATP synthase from *Escherichia coli*. *J. Exp. Biol.* 203:19–28.